Observation of quasiparticle-mediated spin Hall effect in a superconductor

T. Wakamura[1], H. Akaike[2], Y. Omori[1], Y. Niimi[1], S. Takahashi[3], A. Fujimaki[2], S. Maekawa[4,5] and Y. Otani[1,6]

[1]Institute for Solid State Physics, University of Tokyo, Kashiwa 277-8581, Japan

[2]Department of Quantum Engineering, Nagoya University, Nagoya 464-8603, Japan

[3]Institute for Materials Research, Tohoku University, Sendai 980-8577, Japan

[4]CREST, Japan Science and Technology, Tokyo 102-0075, Japan

[5]Advanced Science Research Center, Japan Atomic Energy Agency, Tokai 319-1195, Japan

[6]RIKEN-CEMS, 2-1 Hirosawa, Wako 351-0198, Japan

In some materials the competition between superconductivity and magnetism brings about a variety of unique phenomena such as the coexistence of superconductivity and magnetism in heavy fermion superconductors[1] or spin-triplet supercurrent in ferromagnetic Josephson junctions[2-4]. Recent observations of spin-charge separation in a lateral spin valve with a superconductor[5,6] evidence that these remarkable properties are applicable to spintronics[7], although there are still few works exploring this possibility. Here we report the experimental observation of the quasiparticle-mediated spin Hall effect in a superconductor, NbN. This compound exhibits inverse spin Hall (ISH) effect[8] even below the superconducting transition temperature. Surprisingly, the ISH signal increases over 2000 times compared to that in the normal state with a decrease of the injected spin current. The effect disappears when the distance between the voltage probes becomes larger than the charge imbalance

length[9,10], corroborating that the huge ISH signals measured are mediated by quasiparticles.

Superconductors are expected to show many intriguing phenomena in combination with spintronics, as predicted by previous theoretical studies[7,8,11-14]. One of the distinctive features of superconductors for spintronics is that spin transport in superconductors is mediated not by electrons but by superconducting quasiparticles[7,8,11-13]. Superconducting quasiparticles are superposition of electron-like and hole-like excitation, having spin one-half, and their properties are highly distinct from those of electrons[15]. The quasiparticle-mediated spin current also shows unique phenomena compared with electron-mediated (normal) spin current, such as a dramatic enhancement of the spin relaxation time[11,16,17] or the spin-charge separation[5,6], both of which have already been demonstrated experimentally. However, although the quasiparticle-mediated spin Hall effect (QMSHE) in superconductors is of great interest, it has not yet been demonstrated experimentally despite theoretical predictions[7,8,12,13].

Most importantly, the QMSHE is expected to be enhanced dramatically[7,8,12,13]. The spin Hall effect (SHE) is a phenomenon where a spin current is generated from a charge current through spin-dependent asymmetric scattering due to the spin-orbit interaction (SOI)[18-20]. In its reverse process, i.e. the inverse spin Hall effect (ISHE), a spin current is converted into a charge current through the Onsager reciprocal relation. As importance of spintronics is growing for both science and applications[21], new mechanisms as well as materials for a more efficient conversion between a spin and a change current are highly demanded.

Since spin transport is mediated not by electrons but by quasiparticles in

superconductors, when a spin current is injected into superconductors it is converted into a quasiparticle current via the ISHE. Below the superconducting transition temperature T_C, the superconducting gap Δ opens at the Fermi level, and as temperature decreases Δ grows, thereby the number of quasiparticles decreases. This causes an increase in the resistivity of quasiparticles ρ_{qp} (ref. 22). Since the spin Hall resistivity, a measure of the magnitude of both the SHE and the ISHE, is defined as $\rho_{SHE} = a\rho_{qp} + b\rho_{qp}^2$ (see Supplementary Information for details), the QMSHE and QMISHE are both expected to show a huge enhancement as temperature decreases below T_C.

In order to observe the QMSHE in a superconductor, we used the spin absorption technique, suitable for detecting the SHE and ISHE electrically[19,23]. We fabricated lateral structures[24,25] composed of a ferromagnetic $Ni_{81}Fe_{19}$ (henceforth Py) and a superconducting NbN wire, bridged by a nonmagnetic Cu wire as schematically illustrated in Fig. 1 (for details of the device fabrication, see Methods Summary). NbN is a typical s-wave type-II superconductor[26,27] with a superconducting transition temperature T_C of 10 K for our samples. In this work we pass a current from the Py wire into the Cu wire, away from the NbN superconductor. The resulting spin accumulation in the Cu wire[24,25] diffuses toward the NbN wire, and partly absorbed into the NbN wire because the nonequilibrium spin current is relaxed much faster in the NbN wire than in the Cu wire due to the strong SOI in NbN. This causes a nonzero spin current to flow into the NbN wire.

The spin current injected into the NbN wire is scattered through the ISHE and converted into a charge current. The relation among the generated charge current, a spin of an electron (or quasiparticle) and the injected spin current reads[8]:

$$\mathbf{J}_c \propto \mathbf{J}_s \times \mathbf{s}, \tag{1}$$

where $\mathbf{J}_c$, $\mathbf{J}_s$ and $\mathbf{s}$ denote the charge current vector, the spin current vector and the spin polarization vector of spin current, respectively. Since the spin current is generated from the Py wire (injector), $\mathbf{s}$ is parallel to the magnetization $\mathbf{M}$ of the injector. When the NbN wire is in the superconducting state, the charge current $\mathbf{J}_c$ is replaced by the quasiparticle current $\mathbf{J}_Q$. The detection of $\mathbf{J}_Q$ generated by ISHE is via the charge imbalance effect, which decays in a certain length scale λ_Q from the region where ISHE occurs. The conceptual illustration of QMISHE is shown in Fig. 1 with the relative orientations of $\mathbf{J}_Q$, $\mathbf{s}$ and $\mathbf{J}_s$ when $\mathbf{M}$ is directed parallel to the y-axis along the Cu wire. In the absence of external magnetic field, $\mathbf{M}$ is directed parallel to the x-axis due to the shape anisotropy of Py, and therefore no voltage difference is detected between the two ends of the NbN wire. When an in-plane external magnetic field $\mathbf{H}$ is applied parallel to the y-axis, $\mathbf{M}$ is rotated from the x to the y axis with increasing $\mathbf{H}$. In the equation (1), the right hand side increases as the y component of $\mathbf{s}$ increases, and it reaches a maximum when $\mathbf{s}$ is directed parallel to the y-axis. This condition is fulfilled above the saturation magnetization field H_c of the Py injector because $\mathbf{s}//\mathbf{M}$. In this way, the inverse spin Hall signal strongly depends on the direction of $\mathbf{M}$[19,23].

We first show the observed inverse spin Hall signals at 20 K above T_C (= 10 K). The measurement setup is described in Fig. 2a. Figure 2b shows the inverse spin Hall resistance $R_{ISHE} = V/I$ with applied current I = 300 μA in the upper panel and the anisotropic magnetoresistance (AMR) of the Py injector in the lower panel. It is clear that the signal reflects the magnetization process of Py and saturates above the saturation field of $\mathbf{M}$. The inverse spin Hall signal ΔR_{ISHE} is defined as in the Fig. 2b. The spin Hall angle is negative and estimated to be $\alpha \sim -0.9$ % at 20 K by a three-dimensional analysis[23,28]. The temperature dependence of α_{SHE} in Fig. 2c shows a

linear temperature variation, indicating that intrinsic or side-jump contribution[8] dominates the SHE (see Supplementary Information for details).

Next we cooled the sample down to 3 K much lower than T_C and measured the QMISHE with modulating I. As I decreases, ΔR_{ISHE} dramatically increases for $I < 100$ μA. When $I = 0.01$ μA, the signals show dramatically large values compared with those in the normal state (Fig. 3a). Figure 3b shows the ratio of the QMISHE (ΔR_{ISHE}^{super}) at 3 K to the normal ISHE (ΔR_{ISHE}^{normal}) at 20 K as a function of I. It demonstrates that ΔR_{ISHE} increases with decreasing I and becomes more than 2000 times larger a value than that in the normal state value at $I = 0.01$ μA. We measured the current dependence of ΔR_{ISHE} above T_C, but ΔR_{ISHE} does not depend on I (Fig. 3c). Similar behavior is also observed for other samples from different batches.

In order to confirm that the observed signals originate from the ISHE, we investigated the angular dependence of ΔR_{ISHE}. It follows from the relation (1) that $\Delta R_{ISHE}(\theta)$ at an angle θ between the longitudinal axis of the injector and $\mathbf{H}$ (see the inset of Fig. 3d) is written as

$$\Delta R_{ISHE}(\theta) = \Delta R_{ISHE}(\theta = 90^{\circ})\sin\theta. \tag{2}$$

In Fig. 3d we plot $\Delta R_{ISHE}(\theta)$ normalized by $\Delta R_{ISHE}(\theta = 90^{\circ})$. The experimental results well follow the sinusoidal curve as predicted in equation (2), which also ensures that the observed signals arise from the ISHE.

For obtaining further evidences that quasiparticles mediate the ISHE, we measured the ISHE using samples with a much longer NbN wire. As noted above, when a pure spin current is injected into a superconducting NbN, the QMISHE converts the spin current into a quasiparticle current[7,8,12,13]. Then the quasiparticle current finally relaxes into the Cooper-pair condensates, the process of which accompanies with the

quasiparticle nonequilibrium charge accumulation called the charge imbalance (CI) effect. This CI effect emerges as a spatially dependent electrochemical potential of quasiparticles, which is different from that of the Cooper pairs at a nonequilibrium state and can be detected by normal metal voltage probes weakly coupled to superconductors[7,9,10,29,30]. The CI relaxes in the scale of the CI length λ_Q from the contact region where the ISHE occurs. If the distance d between the voltage probe at the end of the NbN wire (see Fig. 4a) and the contact is much larger than λ_Q, the detected voltage V_{ISHE} disappears because the CI generated by the ISHE decays exponentially with λ_Q (Fig. 4b). We note that all data shown above are taken from the samples with d = 400 nm.

We first show the ISHE signals at 3 K ($< T_C$) with $I = 1$ μA obtained from the samples whose voltage probe distance is $d = 400$ nm ($d1$) and 10 μm ($d2$). We note that while λ_Q for NbN is not available, $d2 = 10$ μm is much larger than λ_Q of typical metallic superconductors[29,30]. As shown in Fig. 4c, the signal for $d = 10$ μm is dramatically suppressed compared with that for $d = 400$ nm, indicating that λ_Q of NbN is much smaller than 10 μm. We also compared the ISHE signals at 20 K and $I = 300$ μA using the same samples. However, both signals, ΔR_{ISHE}, for $d1$ and $d2$ show almost the same value (Fig. 4d). These results also corroborate the detection of the QMISHE in the superconducting NbN mediated by quasiparticles.

In order to explain the enormous QMISHE with decreasing I, we calculated the ISHE signal ΔR_{ISHE} of the superconducting state. The spin Hall resistivity ρ_{SHE} of a superconductor is proportional to ΔR_{ISHE}[8,23];

$$\rho_{SHE} \propto \Delta R_{ISHE},$$

where $\rho_{SHE} = a\rho_{qp} + b\rho_{qp}^2$ with ρ_{qp} being the resistivity of quasiparticles. We note that

the resistivity in the superconducting state may be given by $\rho_{qp} = \rho/[2f_0(\Delta)]$, where $f_0(\Delta)$ is the Fermi distribution function at the superconducting energy gap Δ, because the quasiparticle population is proportional to $[2f_0(\Delta)]$ [22]. We take the value of ρ at 20 K because ρ is almost constant down to the superconducting transition temperature. Based on the previous study[16], we assume that Δ of the NbN is spatial-dependent and substantially suppressed close to the interface with Cu, and that the spin injection current I is proportional to the effective temperature around the Cu/NbN interface. The best fit we obtained is described in Fig. 3b. It well reproduces the enormous enhancement of ΔR_{ISHE} with decreasing I for $I < 10$ µA. We note that our simple theoretical model can explain the experimental results reasonably well for small I region, but it is difficult to fit the data in the whole I region at present (see Supplementary Information for details).

In conclusion, we have experimentally demonstrated for the first time the quasiparticle-mediated SHE (QMSHE) in a superconducting NbN. The inverse spin Hall signal in the superconducting state shows a huge enhancement and becomes more than 2000 times larger than that in the normal state as the spin injection current decreases. The dependence of the signals on the NbN wire length confirms that the ISHE is mediated by superconducting quasiparticles. The dramatically large signal generation from a tiny amount of spin current paves the way to realize a sensitive spin detector with superconductors for a future application.

Methods Summary

Our samples were fabricated by electron-beam lithography, sputtering techniques and electron-beam (EB) evaporations. We first prepared a layer of ZEP520A resist on a

thermally oxidized silicon substrate. After patterning by means of the EB lithography, a 20 nm thick NbN film was reactively sputter-deposited on the substrate. In the sputtering system base pressure was less than 8.0 x 10^{-5} Pa. The NbN layers were deposited by reactive DC-magnetron sputtering in a mixture of Ar and N_2 gases. After the liftoff process we used the EB lithography again and Py was evaporated using an EB evaporator. Then 100 nm of Cu was deposited through a Joule heating evaporator after the same liftoff and the lithography procedures. Before depositions of the Py and the Cu an Ar-ion milling was carried out to make the contacts transparent. The pressure in the chambers was kept below 10^{-9} Torr during the deposition process. The widths of the Py, NbN, and Cu wires are 100 nm, 300 nm and 100 nm, respectively. The transport measurements were performed in a ^{4}He cryostat by using a standard lock-in technique with an ac excitation current of 173 Hz.

1. Matsuda, Y. & Shimahara, H. Fulde-Ferrell-Larkin-Ovchinnikov state in heavy fermion superconductors. *J. Phys. Soc. Jpn*. **76**, 051005 (2007).

2. Keizer, R. S. *et al*. A triplet supercurrent through the half-metallic ferromagnet CrO_2. *Nature* **439**, 825 (2006).

3. Khaire, T. S., Khasawneh, M. A., Pratt, Jr. W. P. & Birge, N. O. Observation of spin-triplet superconductivity in Co-based Josephson junctions. *Phys. Rev. Lett*. **104**, 137002 (2010).

4. Robinson, J. W. A., Witt, J. D. S. & Blamire, M. G. Controlled injection of spin-triplet supercurrents into a strong ferromagnet. *Science* **329**, 59 (2010).

5. Hubler, F., Wolf, M. J., Beckmann, D. & von Lohneysen, H. Long-range spin-polarized quasiparticle transport in mesoscopic Al superconductors with a

Zeeman splitting. *Phys. Rev. Lett.* **109**, 207001 (2012).

6. Quay, C. H. L., Chevallier, D., Bena, C. & Aprili, M. Spin imbalance and spin-charge separation in a mesoscopic superconductor. *Nat. Phys.* **9**, 84 (2013).

7. Takahashi, S. & Maekawa, S. Spin Hall effect in superconductors. *Jpn. J. Appl. Phys.* **51**, 010110 (2012).

8. Takahashi, S. & Maekawa, S. Spin current in metals and superconductors. *J. Phys. Soc. Jpn.* **77**, 031009 (2008).

9. Cadden-Zimansky, P. & Chandrasekhar, V. Nonlocal correlations in normal-metal superconducting systems. *Phys. Rev. Lett.* **97**, 237003 (2006).

10. Cadden-Zimansky, P., Jiang, Z. & Chandrasekhar, V. Charge imbalance, crossed Andreev reflection and elastic co-tunneling in ferromagnet/superconductor/normal-metal structures. *New J. Phys.* **9**, 116 (2007).

11. Yamashita, T., Takahashi, S., Imamura, H. & Maekawa, S. Spin transport and relaxation in superconductors. *Phys. Rev. B* **65**, 172509 (2002).

12. Kontani, H., Goryo, J. & Hirashima, D. S. Intrinsic spin Hall effect in the s-wave superconducting state: analysis of the Rashba model. *Phys. Rev. Lett.* **102**, 086602 (2009).

13. Takahashi, S. & Maekawa, S. Hall effect induced by a spin-polarized current in superconductors. *Phys. Rev. Lett*. **88**, 116601 (1999).

14. Hikino, S. & Yunoki, S. Anomalous enhancement of spin Hall conductivity in a superconductor/normal-metal junction. *Phys. Rev. B* **84**, 020512 (2011).

15. Tinkham M, Introduction to superconductivity 2nd edn (Dover 2004).

16. Wakamura, T. *et al*. Spin injection into a superconductor with strong spin-orbit coupling. *Phys. Rev. Lett*. **112**, 036602 (2014).

17. Yang, H. *et al*., Extremely long quasiparticle spin lifetimes in superconducting aluminum using MgO tunnel spin injectors. *Nat. Mater.* **9**, 586 (2010).

18. Valenzuela, S. O. & Tinkham, M. Direct electronic measurement of the spin Hall effect. *Nature* **442**, 176 (2006).

19. Kimura, T. *et al*. Room-temperature reversible spin Hall effect. *Phys. Rev. Lett*. **98**, 156601 (2007).

20. Saitoh, E., Ueda, M., Miyajima, H. & Tatara, G. Conversion of spin current into charge current at room temperature: Inverse spin-Hall effect. *Appl. Phys. Lett*. **88**, 182509 (2006).

21. Liu, L. Q. *et al*. Spin-torque switching with the giant spin Hall effect of tantalum. *Science* **336**, 555 (2012).

22. Takahashi, S., Yamashita, T., Imamura, H. & Maekawa, S. Spin-relaxation and magnetoresistance in FM/SC/FM tunnel junctions. *J. Mag. Mag. Mater.* **240**, 100 (2002).

23. Niimi, Y. *et al*., Giant spin Hall effect induced by skew scattering from Bismuth impurities inside thin film CuBi alloys. *Phys. Rev. Lett*. **109**, 156602 (2012).

24. Jedema, F. J. *et al*. Electrical detection of spin precession in a metallic mesoscopic spin valve. *Nature* **416**, 713 (2002).

25. Wakamura, T., Ohnishi, K., Niimi, Y. & Otani, Y. Large spin accumulation with long spin diffusion length in Cu/MgO/Permalloy lateral spin valves. *Appl. Phys. Exp*. **4**, 063002 (2011).

26. Shoji, A., Kiryu, S. & Kohjiro, S. Superconducting properties and normal-state resistivity of single-crystal NbN films prepared by a reactive rf-magnetron sputtering method. *Appl. Phys. Lett.* **60**, 1624 (1992).

27. Akaike, H., Funai, T., Naito, N. & Fujimaki, A. Characterization of NbN tunnel junctions with radical-nitrided AlN$_x$ Barriers. *IEEE T. Appl. Supercon.* **23**, 1101306 (2013).

28. Niimi, Y. *et al*. Extrinsic spin Hall effects measured with lateral spin valve structures. *Phys. Rev. B* **89**, 054401 (2014).

29. Arutyunov, K. Yu., Auraneva, H. –P. & Vasenko, A. S. Spatially resolved measurement of nonequilibrium quasiparticle relaxation in superconducting Al. *Phys. Rev. B* **83**, 104509 (2011).

30. Hubler, F., Lemyre, J. C., Beckmann, D. & v. Lohneysen, H. Charge imbalance in superconductors in the low-temperature limit. *Phys. Rev. B* **81**, 184524 (2010).

Author Contributions

T. W. and H. A. fabricated samples. T. W. performed measurements. Analyses are done by T. W. and Y. Omori. Manuscript was prepared by T. W., H. A., Y. N., S. T. and Y. Otani. S. T. and S. M. gave theoretical suggestions. This work is supervised by A. F., S. M. and Y. Otani.

Competing financial interests

The authors declare no competing financial interests.

Figure 1|Schematic image of spin Hall measurement

Ferromagnetic Py wire and superconducting NbN wire are connected by Cu bridge. A pure spin current is generated in the Cu wire by the spin injection current I between the Py and Cu wire. The pure spin current flowing in the Cu is partially absorbed into the NbN wire due to its strong SOI. The absorbed spin current is converted into quasiparticle current $\mathbf{J}_Q$ via the ISHE, creating charge imbalance over the range of λ_Q in the NbN wire. In the conversion region, the direction of $\mathbf{J}_Q$ is determined by the vector product of $\mathbf{s}$ and $\mathbf{J}_S$. The spin-polarization direction $\mathbf{s}$ is controlled by the external in-plane magnetic field $\mathbf{H}$ while the flow-direction of absorbed $\mathbf{J}_S$ is normal to the Cu/NbN interface due to the small spin diffusion length of NbN ($\lambda_{sf} = 7$ nm). In the NbN wire outside the conversion region, quasiparticles are converted into Cooper pairs.

Figure 2|Experimental results of ISHE above T_C

a, Measurement setup for the inverse spin Hall measurement. **b,** Inverse spin Hall signal at $T = 20$ K (top panel) and anisotropic magnetoresistance (AMR) signal of the Py spin injector (bottom panel). The inverse spin Hall signal (ΔR_{ISHE}) is defined as shown in the figure. In-plane magnetic field $\mathbf{H}$ is applied normal to the longitudinal axis of the injector. For all inverse spin Hall signals shown in the figures backgrounds are subtracted from the real data. **c,** Temperature dependence of the spin Hall angle α_{SHE}. The linear relationship of α_{SHE} vs. T indicates the intrinsic or the side-jump contribution. Red dashed line shows the linear fit to the measured α_{SHE}.

Figure 3|ISHE below T_C

a, Inverse spin Hall signal with $I = 0.01$ μA at 3 K (red curve). For comparison we also show the signal at 20 K with $I = 0.01$ μA (blue) and that at 20 K with $I = 300$ μA (green).

b, Spin injection current (I) dependence of the ISHE taken at 3 K. The inverse spin Hall signal taken at 3 K (ΔR_{ISHE}^{super}) is normalized by the value at 20 K (ΔR_{ISHE}^{normal}, $I = 300$ μA). As I decreases, ΔR_{ISHE}^{super} dramatically increases up to more than 2000 times larger than that in the normal state. Blue line shows the calculated relation (see Supplementary Information for details). **c,** Comparison of I dependence of ΔR_{ISHE} normalized by ΔR_{ISHE}^{normal} at 3 K (red squares) and at 20 K (blue squares) in a log-log scale. The orange dashed line is the basis of ΔR_{ISHE}^{normal}, obtained at 20 K with $I = 300$ μA. At 20 K, ΔR_{ISHE}^{normal} is explicitly independent of I. We measured ΔR_{ISHE}^{normal} down to $I = 5$ μA, below which the signal is so small that it is difficult to measure. At 3 K, on the other hand, ΔR_{ISHE} shows a dramatic increase with decreasing I. **d,** Angular dependence of ΔR_{ISHE} at 3 K with $I = 1$ μA. The definition of an angle θ is described in the inset. Plotted data clearly follow the sinusoidal relationship (blue curve) with respect to θ, which ensures that the signals arise from the ISHE. We note that for results shown in *b-d*, each signal is averaged over $|H| > 2000$ Oe, where ΔR_{ISHE} saturates.

Figure 4| NbN length dependence of the observed signals

a, Schematic of a device with distance (length) d between the voltage probe (Cu, shown with brown rectangles) and the contact with the Cu bridge in the NbN wire. **b,** Spatial decay profile of the voltage V_{ISHE} generated by the ISHE as a result of the charge imbalance effect. λ_Q is the charge imbalance length, and $d1$ and $d2$ are a distance from the NbN/Cu contact: $d1 = 400$ nm and $d2 = 10$ μm in our measurements. The measured voltage at $d1$ corresponds to the length of the pink arrow. **c,** Inverse spin Hall signals from the samples with distance of $d1 = 400$ nm (red) and $d2 = 10$ μm (green) at 3 K and 1 μA. To obtain large signals from the sample with $d < \lambda_Q$, the spin injection current (I)

is chosen as 1 µA. Signals for the length of $d2 = 10$ µm are dramatically suppressed while large signals are observed for $d1 = 400$ nm due to the CI effect. **d**, Inverse spin Hall signals taken at 20 K and $I = 300$ µA. Signals show no length dependence.
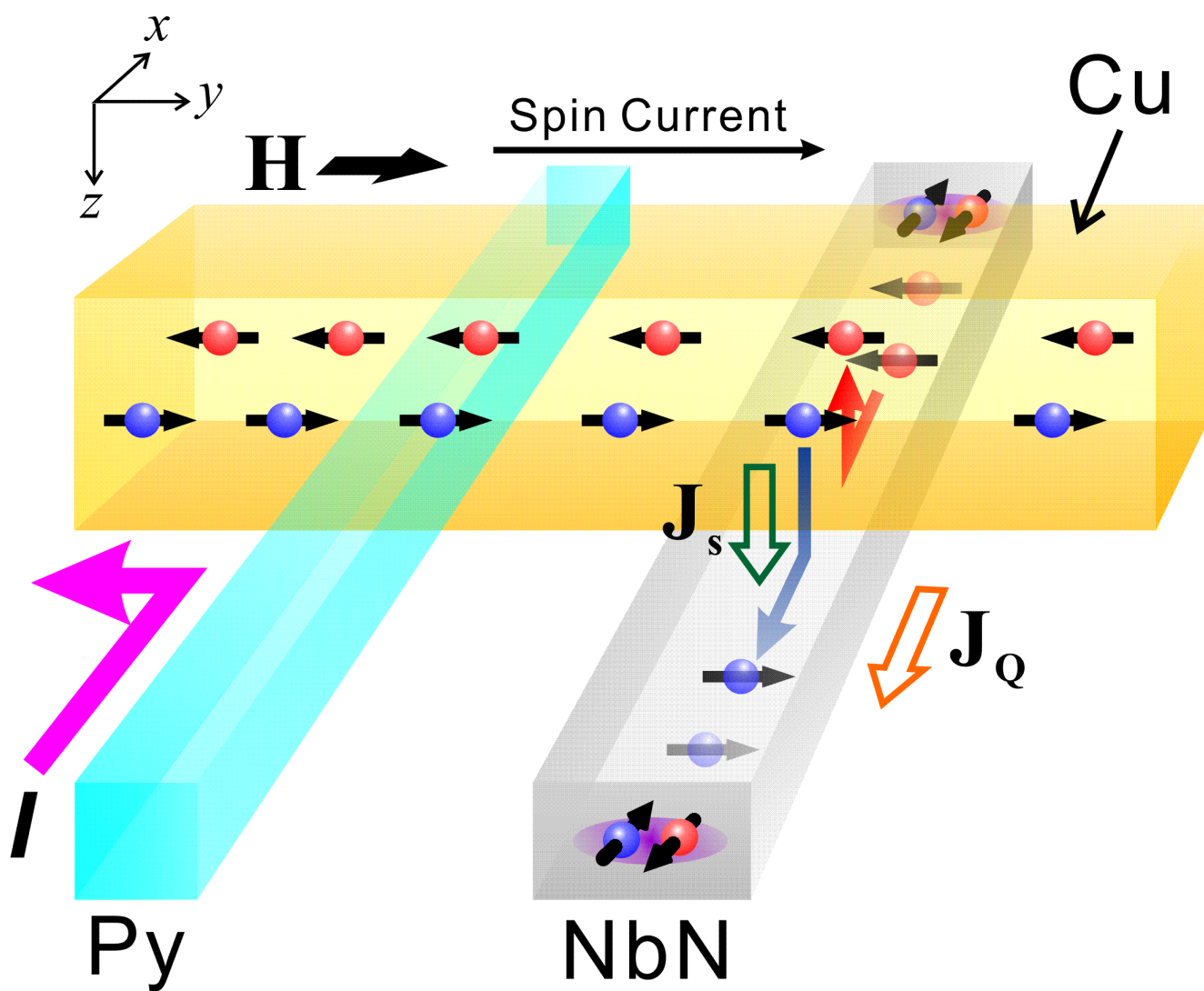
Fig. 1

Fig. 2

Fig. 3

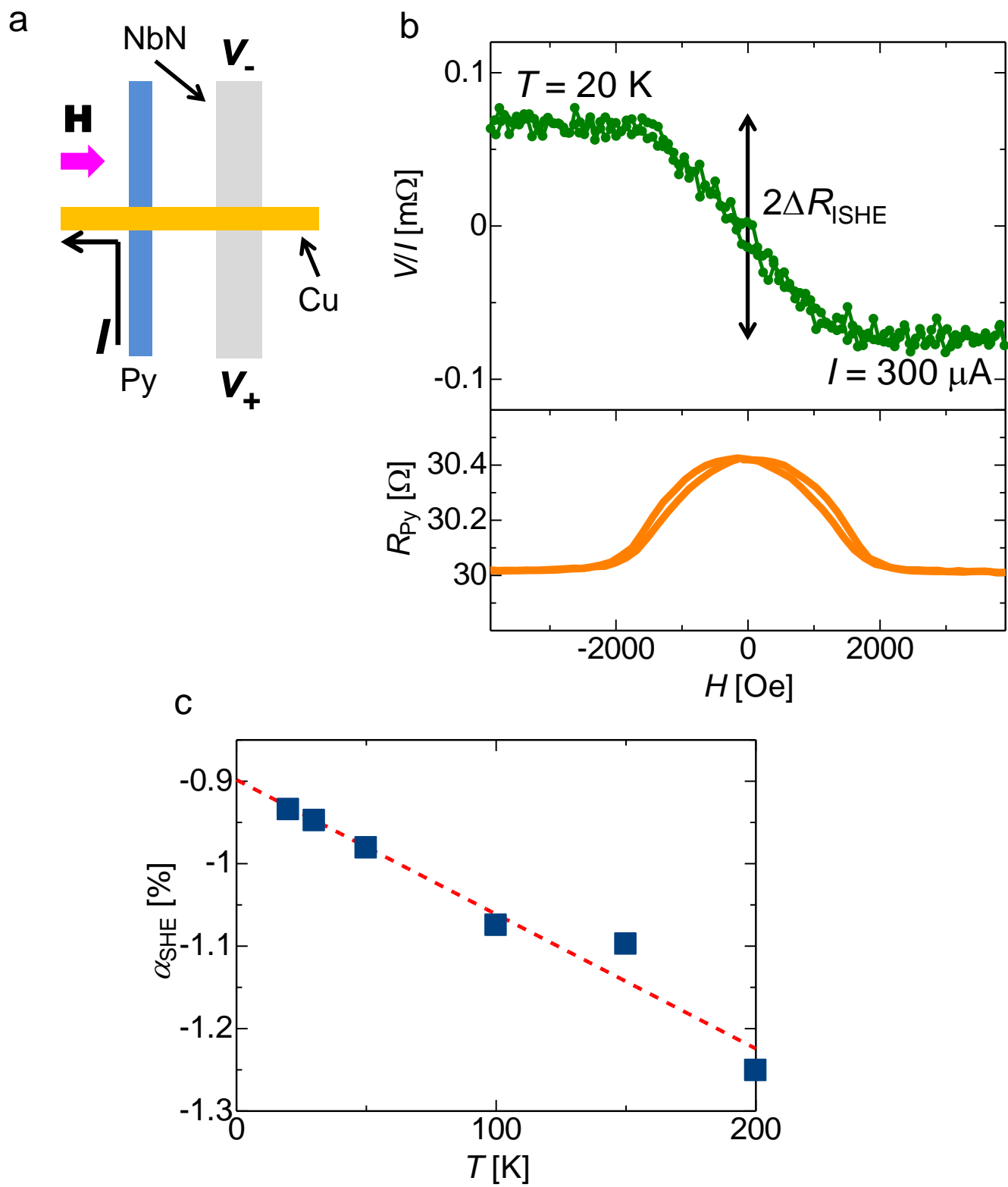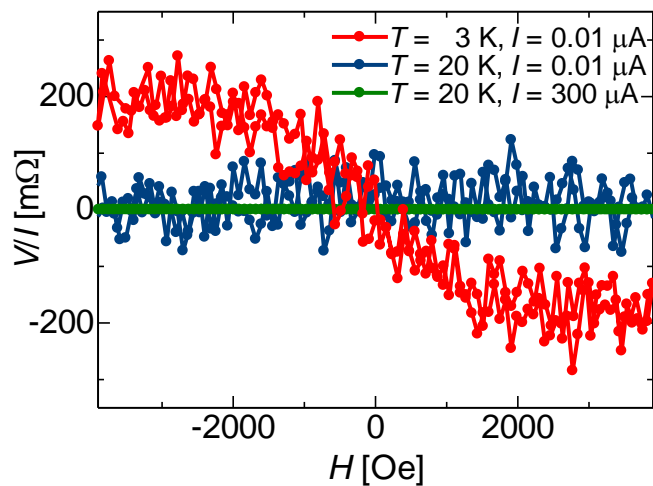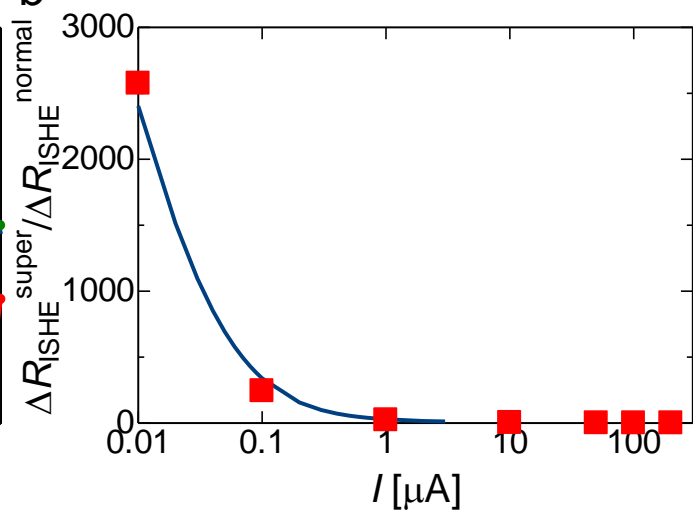Fig. 4

a

V_-

I

$d = d1, d2$

V_+

b

V_{ISHE}

$d2$

$d1$

λ_Q

x

c

$T = 3$ K, $I = 1$ μA

V/I [mΩ]

400 nm (= d1)
10 μm (= d2)

Magnetic Field [Oe]

d

$T = 20$ K, $I = 300$ μA
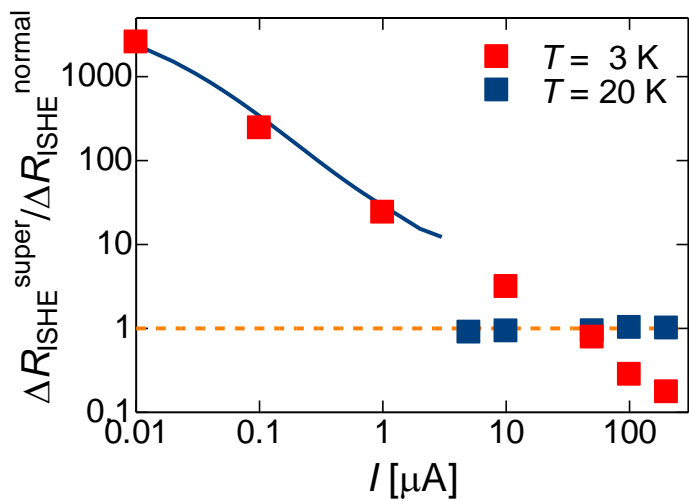
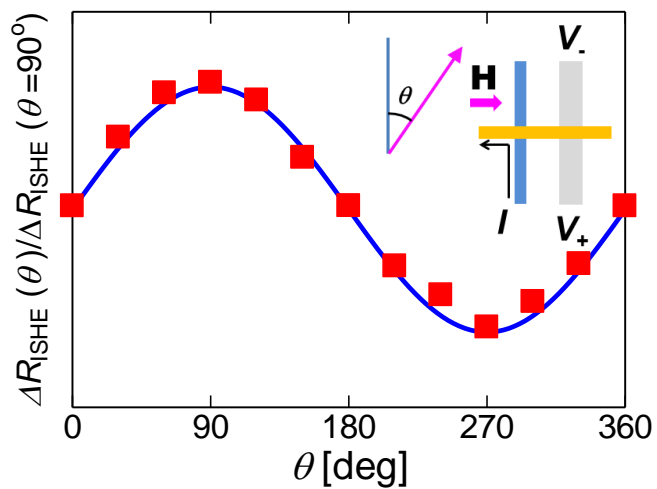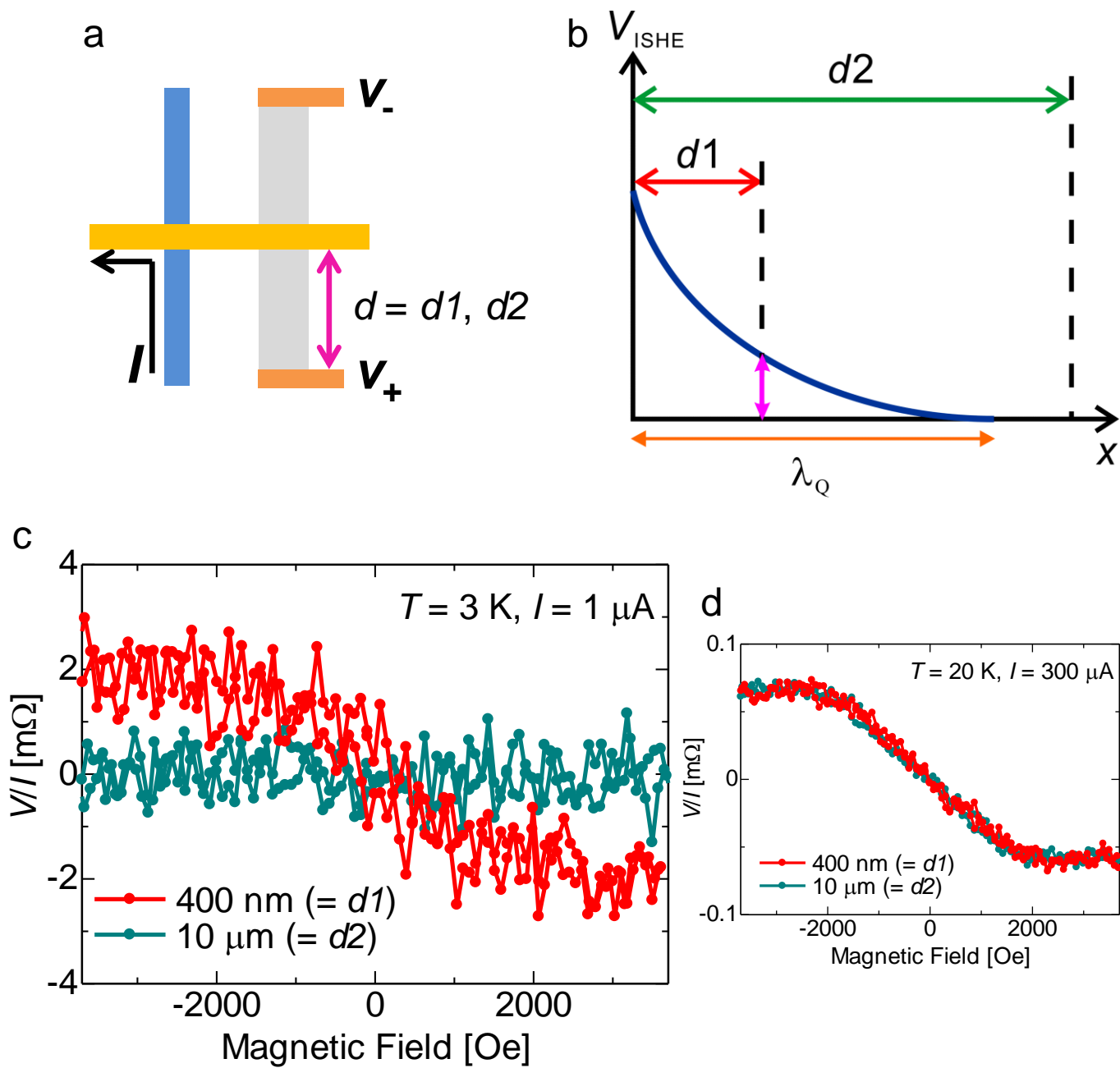V/I [mΩ]

400 nm (= d1)
10 μm (= d2)

Magnetic Field [Oe]

Supplementary Information for "Observation of quasiparticle-mediated spin Hall effect in a superconductor"

T. Wakamura[1], H. Akaike[2], Y. Omori[1], Y. Niimi[1], S.
Takahashi[3], A. Fujimaki[2], S. Maekawa[4,5] and YoshiChika Otani[1,6]

[1]*Institute for Solid State Physics, University of Tokyo, Kashiwa 277-8581, Japan*

[2]*Department of Quantum Engineering,*

Nagoya University, Nagoya 464-8603, Japan

[3]*Institute for Materials Research, Tohoku University, Sendai 980-8577, Japan*

[4]*CREST, Japan Science and Technology, Tokyo 102-0075, Japan*

[5]*Advanced Science Research Center,*

Japan Atomic Energy Agency, Tokai 319-1195, Japan and

[6]*RIKEN-CEMS, 2-1 Hirosawa, Wako, Saitama 351-0198, Japan*

(Dated: February 4, 2015)

S.1 DETAILS OF THE DEVICES

In this section we show the details of the device structure and measurements. Figure 1(a) displays the SEM image of a device. The center-to-center distance between the Py spin injector and the NbN wire is 450 nm. In Fig. 1(b), we show the temperature dependence of resistance of the NbN wire. The coherence length ξ of the NbN wire is estimated to be $\xi = 4$ nm using the relation

$$\xi = \sqrt{\frac{\hbar D}{\Delta_0}}, \tag{1}$$

where the superconducting gap at $T = 0$, Δ_0 is related to T_C as $\Delta_0 = 2.2 k_B T_C$ for a strong coupling superconductor, NbN [31]. We note that the inplane critical field of the NbN wire is larger than ~ 1 T, a maximum field applicable in our system.

S.2 SPIN HALL EFFECT OF NBN ABOVE T_C

The spin Hall effect (SHE) is a nonmagnetic counterpart of the anomalous Hall effect (AHE), which occurs in ferromagnets and has been investigated for many decades. Previous findings for the AHE are also applicable to the SHE; the SHE is attributed to an intrinsic effect and extrinsic effects. The intrinsic effect was first pointed out by Karplus and Luttinger [32] in the concept of the anomalous velocity, and arises from the band structure of perfect
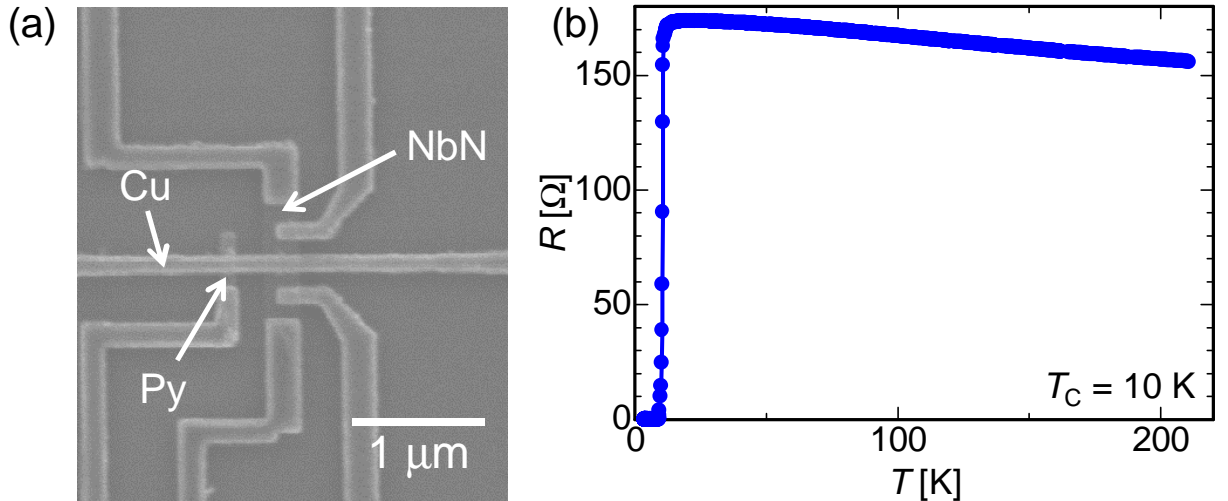

FIG. 1. (a): SEM image of a device. (b): Resistance of the NbN wire (R) as a function of temperatuire (T).

crystals. It is characterized by a finite value of an integrated Berry phase curvature in the momentum space [33]. Previous studies on the AHE demonstrate that when the intrisic effect is dominant, the relation between the Hall resistivity ρ_{yx} (or the spin Hall resistivity ρ_{SHE} in the SHE) and the longitudinal resistivity ρ_{xx} is $\rho_{yx} \propto \rho_{xx}^2$ in moderately resistive metals [34]. The extrinsic effects are, on the other hand, relevant to disorder scatterings in imperfect crystals. There are two contributions to the extrinsic effects; the skew-scattering (SS) [35] and the side-jump (SJ) [36] effect. The SS contribution arises from spin-asymmetric scatterings by impurities with strong spin-orbit interaction. When the SS is dominant, one obtains the relation $\rho_{yx} \propto \rho_{xx}$. The SJ effect brings the anomalous velocity to electrons thus the electrons move transversely when scattered. In this regime $\rho_{yx} \propto \rho_{xx}^2$. Taking these three contributions into account, ρ_{yx} can be expressed as

$$\rho_{yx} = a\rho_{xx} + b\rho_{xx}^2, \tag{2}$$

where both a and b are constant. We note that we follow the conventional relation between ρ_{yx} and ρ_{xx} in (2) and do not replace ρ_{xx} with ρ_{imp} for the extrinsic contributions as done in [37], where ρ_{imp} is a temperature independent impurity resistivity. This is because in our system we cannot explicitly distinguish the extrinsic effects from the intrinsic effect. The Hall angle (or the spin Hall angle), defined as $\alpha_{\text{H}}(\alpha_{\text{SHE}}) \equiv \rho_{yx}(\rho_{\text{SHE}})/\rho_{xx}$, is thus written as

$$\alpha_{\text{H}} = a + b\rho_{xx}. \tag{3}$$

As shown in Fig. 1(b), above $T_{\text{C}}(=10\text{ K})$ one can see the linear relation between R (namely, ρ_{xx}) and T. In the main part of our paper we show that the spin Hall angle α_{SHE} is proportional to T. Thus by using these two relations we can determine two constants a and b.

S.3 RELATION BETWEEN THE SPIN INJECTION CURRENT I AND THE EFFECTIVE TEMPERATURE AT THE CU/NBN INTERFACE

In order to confirm that superconductivity is sustained in the NbN wire close to the interface with the Cu bridge, we measured the temperature (T) dependence and spin injection current (I) dependence of the resistance of the NbN. The results are shown in Fig. 2 with the measurement setup in the inset. R_{I} is defined as V/i ($V \equiv (V_+ - V_-)$) with i the
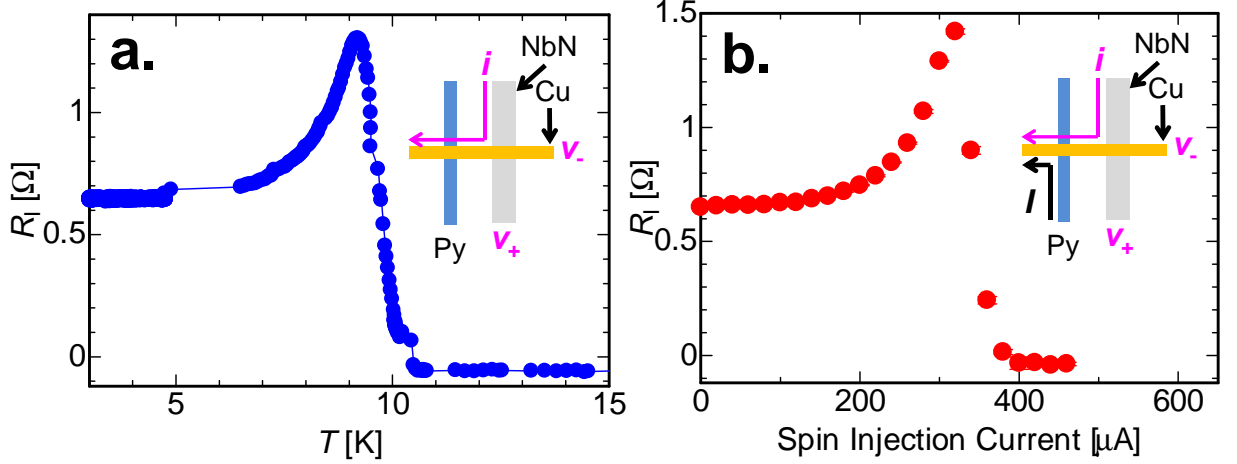
FIG. 2. **a.** Temperature dependence of the interface resistance $R_I \equiv V/i$, $V = V_+ - V_-$. **b.** Spin injection current (I) dependence of R_I. Insets show the measurement setup.

bias current. As for the temperature dependence, when $T > T_C$, $R_I < 0$, originated from current inhomogeneities at the transparent Cu/NbN interface [38, 39]. At $T = T_C$, a peak structure appears, and extra resistance is added for $T < T_C$ (Fig. 2a). They originate from the charge imbalance effect, a nonequilibrium phenomenon relevant to superconductivity of the NbN, as observed in the previous studies [40, 43]. When we fixed T and modulating I, we obtained exactly the same curve as the temperature dependence of R_I (Fig. 2b). In our previous work [40], we observed the same correspondance between T and I dependence of the resistance close to the superconductor/normal metal interface, and by comparing these two curves, we can estimate the effective temperature at the superconductor/normal metal interface for a certain I. In this study, we can also apply the same way to evaluate the effective temperature at the Cu/NbN interface, which is modulated through I.

To acquire the relation between I and the effective temperature it is necessary to consider the Wiedemann-Franz law and determine temperatures for electrons, phonons and the substrate, and also the coupling constants among them as discussed in [41]. We estimated the temperature difference in the Cu bridge between the Py spin injector and the NbN wire based on the Wiedemann-Franz law, and found that the temperature difference is negligibly small (< 0.1 K). We next evaluate the temperature difference between electrons and phonons. We note here that our measurements are performed above 3 K. As many previous studies on the temperature dependence of the phase coherence time in metals revealed [42], from 3 K and above the dephasing due to the electron-phonon coupling becomes more important

4

than that due to the electron-electron interaction. Therefore the phonon temperature cannot be decoupled from the electron temperature, indicating that the same temperature for electrons and phonons can be assumed. As for the thermal coupling between the substrate and phonons, the Kapitza resistance becomes significant at low temperatures as pointed out in [41]. However, in the present case measurements are done at much higher temperatures than those in [41], thus the Kapitza resistance is not so critical.

Taking into accout these facts, to calculate the relation between I and the effective temperature, we used a simple model. We first consider the temperature dependence of the energy density per unit volume, which is obtained by integrating the temperature dependence of the heat capacity of a material, as

$$\varepsilon = \gamma T^2 + A T^4, \tag{4}$$

where γ is the electronic heat capacity and A is the heat capacity of phonons [45]. We assume here that the electronic temperature and the phonon temperature are the same $(=T)$ based on the above considerations. As a heat source, we assume that main contribution is from the Py wire, which has much larger resistance than that of the Cu wire. When a current I flows in a wire with a resistance R for time t, we have the Joule heating thus thermal energy is

$$Q = R I^2 t, \tag{5}$$

where R is the resistance of the Py and t is the duration for electrons to pass through the Py wire. Taking into account the diffusive transport, t can be written as

$$t = \frac{L_{\mathrm{Py}}^2}{D}, \tag{6}$$

with the diffusion constant D of Py and the length L_{Py} of the Py spin injector (in the present case $L_{\mathrm{Py}} = 90$ nm). D is estimated to be $D = 2.0$ cm^{2}s^{-1} by using the Einstein's relation $\sigma = e^2 N(0) D$ with the conductivity of Py $\sigma = 5 \times 10^6$ Ω^{-1}m^{-1} and the density of the states at the Fermi energy $N(0) = 1.0 \times 10^{48}$ J^{-1} m^{-3} [44]. Associating Eq. (5) with the net increase of the energy density:

$$\Delta\varepsilon = \gamma(T^2 - T_0^2) + A(T^4 - T_0^4), \tag{7}$$

where T_0 is the enviromental temperature, then we can write

$$I^2 = \frac{\gamma V}{Rt}(T^2 - T_0^2) + \frac{AV}{Rt}(T^4 - T_0^4), \tag{8}$$
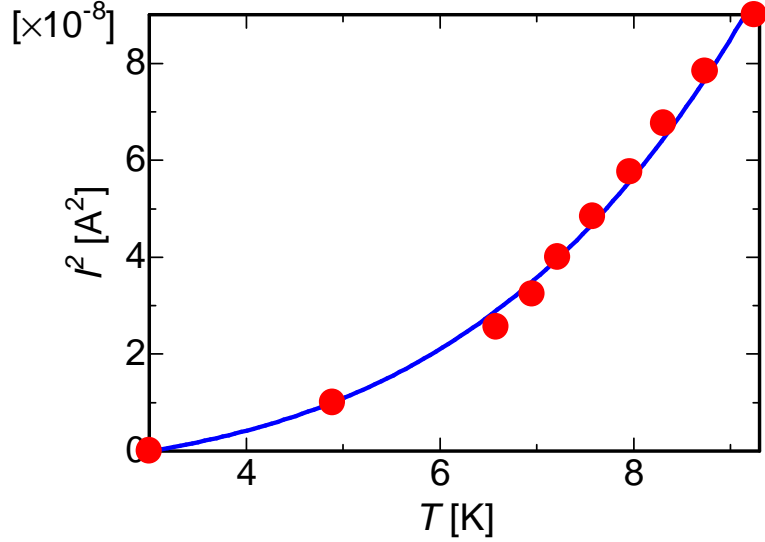
FIG. 3. I^2 as a function of T from the experimental results with the fitting curve calculated based on (8).

where V is the volume of the Cu bridge which mediates the heat flow. We show in Fig. 3 the experimental results on the relation between I^2 and the effective temperature with the fitting curve based on the equation (8). The curve reproduces the experimetal data fairly well, and we can obtain $\gamma = 64$ J-m^{-3}-K^{-2} and $A = 5.1$ J-m^{-3}-K^{-4}. These values are very close to the value from the reference $\gamma = 94$ J-m^{-3}-K^{-2} and $A = 8.7$ J-m^{-3}-K^{-4} [45], indicating the validity of our model to estimate the effective temperature at the Cu/NbN interface. By using this method we can determine T for each I. In the next section we discuss the details of the calculations for the inverse spin Hall signals considering this relation between T and I.

S.4 DETAILS OF THE CALCULATION FOR THE ABSORBED SPIN CURRENT INTO THE NBN

In order to reproduce the enormous enhancement of the inverse spin Hall signals below T_C, we show the details of the calculation which relates the superconductivity of the NbN to the SHE. From the previous studies, the relation between the spin Hall resistivity ρ_{SHE} and the inverse spin Hall signal within the one-dimensional model is expressed as [46]

$$\rho_{SHE} = \frac{w_M}{\zeta} \left(\frac{I}{I_s} \right) \Delta R_{ISHE}, \tag{9}$$

6

where w_{M}, ζ and I_{s} represent the width of the NbN wire, a shunting factor and a spin current injected into the NbN wire, respectively [46].

As discussed in S.1, ρ_{SHE} is expressed with ρ_{xx} as

$$\rho_{\mathrm{SHE}} = a\rho_{xx} + b\rho_{xx}^2. \tag{10}$$

It is important to note that in the superconducting state it is necessary to replace ρ_{xx} to ρ_{qp}, the resistivity of quasiparticles. In the theoretical studies it is found that ρ_{qp} can be expressed with ρ_{xx} as $\rho_{\mathrm{qp}} = \rho_{xx}/[2f_0(\Delta)]$, where $f_0(\Delta) = (\exp(\Delta/k_{\mathrm{B}}T) + 1)^{-1}$ is the Fermi distribution function at the superconducting gap Δ of the NbN [47]. Then from (9) and (10), we obtain

$$\Delta R_{\mathrm{ISHE}} = \left(\frac{I_{\mathrm{s}}}{I}\right) \frac{\zeta}{w_{\mathrm{M}}} \left(a\frac{\rho_{xx}}{2f_0(\Delta)} + b\left(\frac{\rho_{xx}}{2f_0(\Delta)}\right)^2\right) e^{-\frac{d}{\lambda_{\mathrm{Q}}}}. \tag{11}$$

In the above equation effects from superconductivity are taken into account via $f_0(\Delta)$. Since the ISHE is observed via the charge imbalance effect, the measured signals are dependent on the distance between the voltage probe and the Cu/NbN junction. To take this into account, we include the decay of the charge imbalance effect with a factor $e^{-\frac{d}{\lambda_{\mathrm{Q}}}}$, where λ_{Q} is the charge imbalance length and d is the distance between the Cu/NbN junction and the edge of the NbN wire. Due to the transparent contact between the Cu/NbN interface in our device, the superconducting gap Δ is suppressed close to the interface because of the superconducting proximity effect [48]. Thus in calculating $f_0(\Delta)$ we assume that Δ is spatially dependent as $\Delta(x) = \Delta_0 x/\xi$, where Δ_0 is the bulk gap of the NbN and ξ is the superconducting coherence length. We take $x = 0$ at the Cu/NbN interface and $x > 0$ in the NbN, with the x axis normal to the interface. We confirmed that the spatial evolution of Δ does not affect our final results drastically. As seen in Fig. 1(b), ρ_{xx} is almost constant for $T_{\mathrm{C}} < T < 20$ K, thus we take in this temperature range $\rho_{xx} = \rho_{xx}(T = 20 \text{ K}) \equiv \rho_{\mathrm{imp}}$, and $\rho_{\mathrm{qp}} = \rho_{\mathrm{imp}}/[2f_0(\Delta)]$. Then the ratio of ΔR_{ISHE} in the superconducting to the normal (at 20 K) states for a certain I becomes

$$\frac{\Delta R_{\mathrm{ISHE}}^{\mathrm{super}}}{\Delta R_{\mathrm{ISHE}}^{\mathrm{normal}}} = \left(\frac{I_{\mathrm{s}}^{\mathrm{super}}}{I_{\mathrm{s}}^{\mathrm{normal}}}\right) \frac{\zeta^{\mathrm{super}}}{\zeta^{\mathrm{normal}}} \left(\frac{a(\rho_{\mathrm{imp}}/2f_0(\Delta)) + b(\rho_{\mathrm{imp}}/2f_0(\Delta))^2}{a\rho_{\mathrm{imp}} + b\rho_{\mathrm{imp}}^2}\right) e^{-\frac{d}{\lambda_{\mathrm{Q}}}}. \tag{12}$$

The term $I_{\mathrm{s}}^{\mathrm{super}}/I_{\mathrm{s}}^{\mathrm{normal}}$ can be described as [40]

$$\frac{I_{\mathrm{s}}^{\mathrm{super}}}{I_{\mathrm{s}}^{\mathrm{normal}}} = \int_{-\infty}^{\infty} n_{\mathrm{S}}(E) \left(-\frac{\partial f_0(E)}{\partial E}\right) dE, \tag{13}$$

7

where $n_S(E)$ is the density of the states of the NbN wire. We found from the temperature dependence of α_H and ρ_{xx}, $|b/a| \sim 10^6~\Omega^{-1}\text{cm}^{-1}$. Thus hereafter we only consider the term quadratic in ρ_{imp}. From the relation between I and T in Eq. (8), we performed calculation assuming $\Delta T (\equiv T - T_0) \propto \sqrt{I}$, and obtained the relation between $\Delta R_{\text{ISHE}}^{\text{super}}/\Delta R_{\text{ISHE}}^{\text{normal}}$ and I, as shown by the solid curve in Fig. 3b and Fig. 3c in the main text. In the analysis we used $\rho_{\text{imp}} = 220~\mu\Omega\text{cm}$ and $\zeta^{\text{super}}/\zeta^{\text{normal}} = 4$ taking into account higher resistivity of NbN than CuIr in [46]. We numerically calculated (12) and (13) at each x, and finally the results were averaged over x. We note that the calculation can reproduce well the experimental data in the small I regime ($I < 10~\mu\text{A}$), but it fails when I is larger. This might stem from the difference between the relation $\Delta T \propto \sqrt{I}$ and that obtained from (8). The present model is not complete enough to explain the behavior of the inverse spin Hall signal in the whole I region. It is possible that effects other than the effective temperature increase also play a role, thus more elaborated models are necessary to reproduce all experimental data. Since as I increases, T also increases, the deviation of the theoretical calculations from the experimental data might be related to the anomalous temperature dependence of ΔR_{ISHE} close to T_C as we will discuss in the next section.
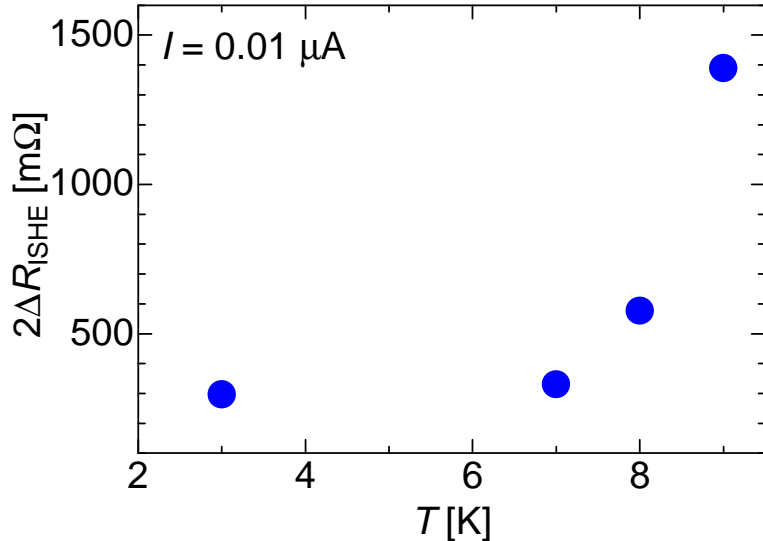

FIG. 4. Temperature dependence of the ISHE signal ($2\Delta R_{\text{ISHE}}$) below T_C.

S.5 TEMPERATURE DEPENDENCE OF THE ISHE SIGNALS

We finally show the temperature dependence of ΔR_{ISHE} below T_{C}. As T is approaching to T_{C}, we observed diverging ISHE signals, which are not taken into account in the previous theories [49, 50]. We note a strong resemblance between the charge imbalance (CI) effect and the inverse spin Hall signal near T_{C}. Therefore diversing ΔR_{ISHE} might be associated with the divergence of the CI at $T = T_{\mathrm{C}}$. However, it is also possible that nonequibrium superconductivity plays an important role [52]. For future studies, it is necessary to obtain a clear relation between the spin injection current and the temperature and also to elucidate the origin of this anomalous T dependence of the inverse spin Hall signals based on more experimental data and elaborate models.

S.6 BASELINE RESISTANCE IN THE ISHE SIGNALS

For the figures in the main text, the baseline resistance (backgrounds) is subtracted from the raw data. The baseline resistance in nonlocal setup is ideally zero, but it always appears in real measurements. Its origins are often discussed in many studies, and several possible candidates are proposed for nonlocal measurements with spin valves, such as current inhomogeneity at the ferromagnet/nonmagnet interface [53] or thermal effects [54]. However, none of them are conclusive and the origin of the baseline resistance is still an open question. The baseline resistance also appears in our measurements regardless of the NbN in the normal or superconducting state, and its magnitude and sign depend on devices. We note that the existence of the backgrounds does not affect the inverse spin Hall signals.

———

[31] Shoji, A., Kiryu, S. and Kohjiro, S. Superconducting properties and normal-state resistivity of single-crystal NbN films prepared by a reactive rf-magnetron sputtering method. Appl. Phys. Lett. **60**, 1624 (1992).

[32] Karplus, R. and Luttinger, J. M. Hall effect in ferromagnetics. Phys. Rev. **95**, 1154 (1954).

[33] Nagaosa, N. *et al.* Anomalous Hall effect. Rev. Mod. Phys. **82**, 1539 (2010).

[34] Onoda, S., Sugimoto, N. and Nagaosa, N. Intrinsic versus extrinsic anomalous Hall effect in ferromagnets. Phys. Rev. Lett. **97**, 126602 (2006).

[35] Smit, J. The spontaneous Hall effect in ferromagnetics 1. Physica **21**, 877 (1955).
Smit, J. The spontaneous Hall effect in ferromagnetics 2. Physica **24**, 39 (1958).

[36] Berger, L. Side-jump mechanism for the Hall effect of ferromagnets. Phys. Rev. B **2**, 4559 (1970).

[37] Tian, Y., Ye, L. and Jin, X. Proper scaling of anomalous Hall effect. Phys. Rev. Lett. **103**, 087206 (2009).

[38] Pomeroy, J. M. and Grube, H. J. Negative resistanceh errors in four-point measurements of tunnel junctions and other crossed-wire devices. J. Appl. Phys. **105**, 094503 (2009).

[39] Moodera, J. S. *et al.* Geometrically enhanced magnetoresistance in ferromagnet-insulator-ferromagnet tunnel junctions. Appl. Phys. Lett. **69**, 708 (1996).

[40] Wakamura, T. *et al.* Spin injection into a superconductor with strong spin-orbit coupling. Phys. Rev. Lett. **112**, 036602 (2014).

[41] Henny, M. *et al.* 1/3-shot-noise suppression in diffusive nanowires. Phys. Rev. B **59**, 2871 (1999).

[42] Mallet, F. *et al.* Scaling of the low-temperature dephasing rate in Kondo systems. Phys. Rev. Lett. **97**, 226804 (2006).

[43] Cadden-Zimansky, P. and Chandrasekhar, V. Nonlocal correlations in normal-metal superconducting systems. Phys. Rev. Lett. **97**, 237003 (2006).

[44] Papaconstantpoulos, D. A., in *Handbook of the Band Structure of Elemental Solids* (Plenum, New York, 1986).

[45] Ashcroft, N. W. and Mermin, N. D. in *Solid State Physics* Ch2 (Saunders College, 1976).

[46] Niimi, Y. *et al.* Extrinsic spin Hall effect induced by iridium impurities in Cu. Phys. Rev. Lett. **106**, 126601 (2011).

[47] Takahashi, S., Yamashita, T., Imamura, H. and Maekawa, S. Spin-relaxation and magnetoresistance in FM/SC/FM tunnel junctions. J. Mag. Mag. Mater. **240**, 100 (2002).

[48] Buzdin, A. I. Proximity effects in superconductor-ferromagnet heterostructures. Rev. Mod. Phys. **77**, 935 (2005).

[49] Takahashi, S. and Maekawa, S. Spin Hall effect in superconductors. Jpn. J. Appl. Phys. **51**, 010110 (2012).

[50] Kontani, H., Goryo, J. and Hirashima, D. S. Intrinsic spin Hall effect in the s-wave superconducting state: analysis of the Rashba model. Phys. Rev. Lett. **102**, 086602 (2009).

[51] Mamin, H. J., Clarke, J. and Van Harlingen, D. J. Charge imbalance induced by a temperature gradient in superconducting aluminum. Phys. Rev. B **29**, 3881 (1984).

[52] Langenderg, D. N. and Larkin, A. in *Non-Equilibrium Superconductivity* (North-Holland, Amsterdam, 1980).

[53] Johnson, M and Silsbee, R. H. Calculation of nonlocal baseline resistance in a quasi-one-dimensional wire. Phys. Rev. B **76**, 153107 (2007).

[54] Bakker, F. L., Slachter A., Adam, J. -P and van Wees, B. J. Interplay of Peltier and Seebeck effects in nanoscale nonlocal spin valves. Phys. Rev. Lett. **105**, 136601 (2010).